Electromagnetic Pigging System based on Sandwich Differential Planar Coil

Yupei Yang, Bin Gao*, Dong Liu, Qiuping Ma, Haoran Li, Wai Lok Woo, Gaige Ru

***Abstract*—In-pipeline inspection is an important pre-control method to ensure the safety of oil and gas pipeline transportation. This paper proposes an electromagnetic in-pipe detector based on passive resonance-enhanced differential planar coils to detect defects on the inner surface of pipes. Both qualitative and quantitative analysis of pipeline defects and damage are developed. The introduction of passive resonant coils is shown to significantly improve the detection capability of the sensor. This is coupled with the establishment of a theoretical derivation model of the proposed structure. The hardware platform of the laboratory system has been built, and an eddy current internal detector suitable for 8-inch diameter pipes is developed and integrated into the system. Numerical simulations and experimental verifications on flat defects and pipe defects have been undertaken. The obtained results have shown that the real defects have been correctly detected and that the system is effective. reliable and efficiency.**

***Index Terms*—Eddy current testing, In-pipeline inspection, Planar coil, resonance enhancement.**

I INTRODUCTION

With the continuous improvement in industrialization, huge demands becomes more prevalent for non-destructive, non-invasive, and non-contact diagnostic mechanism in maintaining pipeline integrity. There are huge oil and gas pipelines in the world and statistics [1] show that the accident rate due to the defects of pipelines is on the rise [2]. Hazards such as cracks, dents, metal loss, or corrosion that occur on the pipe may cause personal injury or death, economic loss, and environmental damage [3]. Thus, correct detection and timely monitoring of pipeline integrity before failure is essential for production and security.

Internal or inline inspection (ILI) technology is recognized as the most effective method for detecting and locating pipeline defects [4][5][6][7]. It moves in the pipeline through non-destructive testing (NDT) methods, such as magnetic flux leakage (MFL), ultrasonic testing (UT), and eddy current (EC) which are equipped with pipeline inspection instruments (PIG) [8], potential defective areas were identified after evaluating data [9]. Over the years, in-pipe inspections have been intensified. For example, three-axis high-resolution magnetic flux leakage inspection, liquid ultrasonic crack inspection, electromagnetic acoustic transducer (EMAT) inspection, and remote field eddy current (RFEC) inspection technologies are proposed to achieve high detection accuracy of pipe defects [10]. In 1965, the American Tuboscope company used the magnetic flux leakage detection method to detect the pipeline [11]. This was the first pipeline inspection tool. MFL PIG is the most frequently used in-line inspection tool. Shenyang University of Technology, Pipetel company, GE PII company, and T.D.W company have already developed PIG and successfully tested it in the gas pipeline. The research team from Shenyang University of Technology focuses on the large diameter gas pipeline inspection and developed a full range of ultra-high-definition magnetic flux leakage detectors. They used the finite element method to calculate the influence of magnetic field intensity for defect detection. A high-speed magnetic flux leakage detection experimental platform was developed to carry out experimental research on steel pipe defects under different operating speeds and different external magnetic field intensity [12]. Pipetel company developed "EXPLORER ILI fleet" for the inspection of 6- to 36-inch diameter natural gas and liquid pipelines. This tool can move in two directions in the pipeline and enables visual as well as non-destructive inspection with multipoint data collection. SpirALL Magnetic Flux Leakage (SMFL) is introduced to explore the advantage based on the spiral magnetic leakage structure while it complements the insufficient of a single axial magnetic field. The Magnetic Scan MFL detector developed by GE PII company is suitable for the pipe diameter range of 76-1422 mm. The high field "Speed-stable" magnetizer enables the detection speed of reaching 5 m/s and 216 Hall effect sensors are integrated for high-resolution detection. EC is useful for crack detection and material thickness measurements. It can adapt to wider temperature range for operation and its advantages consist of smaller size, lightweight, and relatively lower cost. Rosen company is dedicated to corrosion detection and heavy-walled pipeline inspection with eddy current testing. It has developed a pipeline eddy current internal detector for metal loss, which is combined with a deflection sensor that allows for simultaneous measurement of the inner pipeline contour. Thus, not only corrosion but also deformations can be captured in one run. Many types of eddy current probes are dedicated to surface defects, especially the application of Planar-type probes. Yamada et al. [13] presented a dual planar micro coil structure

to reduce the noise and improve the strength of the measured signal. It discussed the relationships between Resonance frequency and defect detection signal-to-noise ratio. Fava et al. [14] calculated the fields produced by planar rectangular spiral coils through the second-order vector potential formulation and impedance plane diagrams with different frequencies, lift-off, and half-space conductivity. Xu et al. [15] investigated an ECT probe composed of double uneven step distributing planar coil. The location of cracks on the metal surface can be detected in non-scanning detection mode while the lift-off should be no more than 1.9 mm. Recently, a planar coil has been used flexibly in various fields. Rosado et al. [16] presented a new planar eddy current probe that can dynamically modify the induced eddy currents pattern. It is good for detecting cracks in different orientations. Pasadas et al. [17] excited a double-layer planar coil to generate a rotating magnetic field and received it by giant magnetoresistive (GMR) sensor to detect a particular kind of machined cracks with complex geometry. Machado designed a new planar ECT array probe to detect unidirectional carbon fiber reinforced polymer (UD CFRP) materials at both high lift-off (up to 3 mm) and velocity (up to 4 m/s) [18]. With customized TMR sensors and application-specific integrated circuits (ASICs) for signal processing and interface, Caetano et al. [19]disclosed two non-destructive testing probes, one for surface defects and the other for buried defects. Through customized TMR sensors and application-specific integrated circuits (ASICs) for signal processing and interface. However, it is mainly used in the laboratory environment at present, and since the lift-off height is low, it is difficult to detect defects in the actual pipeline environment. In our paper, a new differential sensing structure based on matching capacitors and passive enhancement coils is proposed. Planar coils have shown to contain the capability of good detection performance in eddy current nondestructive testing. The differential structure can reduce the lift-off impact as well as the influence of the external environment such as temperature. The excitation coil adopts rectangular symmetry to form a uniform eddy current field in the middle of the coil. The multi-layer structure of the receiving coil can increase the sensitivity of the detectability. The proposed passive enhancement coil adds a coupling path between the excitation coil, the receiving coil, and the test piece, which enhances the sensitivity of detection. In particular, the capacitance of the receiving coil is adjusted to significantly enlarge the varying amplitude. In particular, we have integrated the proposed probe array with pipeline “PIG”. Both simulations and experiments have demonstrated the feasibility of the proposed sensing structure.

The rest of the paper is organized as follows: Section II presents the resonance enhancement effect based on the magnetic coupling mutual inductance model and introduces the complete detection system. Section III conducts a finite element simulation with the designed model, and presents the experiment results and analysis. Finally, the conclusion is drawn in Section IV

II PROPOSED METHODOLOGY

A. Proposed Passive Enhanced Eddy Current Probe and Pipeline Inspection System

The proposed detection system is illustrated in Fig.1(a) and (b). Fig.1(a) shows the test system for the detection ability of the probe on the plate under experimental conditions. The Function generator device generates a sine wave of a specific frequency, and the power amplifier is required to increase its output current. The eddy current coil is excited by the excitation device which constitutes the AC signal. Data acquisition card collects sensor data, and PC performs data processing. The Eddy current pipe pig is shown in Fig.1(b). The Eddy current pipe pig adopts an integrated petal structure. Also, the eddy current sensor is encapsulated in the petal, and the hardware system is placed in the middle cavity of the In-pipe detector.

The structure of the Pipe pig is shown in Fig.1(b). There are 20 measurement channels. The size of the in-pipe detector corresponds to the size of the pipe to be inspected. The hardware system is mainly composed of FPGA, MCU, AD/DA conversion, power amplifier, and amplitude extraction. The FPGA generates two signals through the DAC, one as the excitation signal, and the other as the reference signal. It extracts the amplitude and phase of the signal, and the ADC collects the signal after the extraction. The MCU stores the data sent by the FPGA and communicates with the host computer to complete the data storage and real-time display.

The diagram of the eddy current sensor structure is shown in Fig. 2. The eddy current sensor consists of three particular parts: (i) a differential rectangular excitation coil, (ii) a four-layer passive enhancement coil with a parallel capacitor in the middle, and (iii) a four-layer rectangular receiving coil. The excitation coil adopts a differential rectangular structure, which can not only generate a uniform eddy current field but also reduce the influence of lift-off and interference. The design of the multi-layer receiving coil is built to increase the number of turns of the receiving coil for improving detectability. The passive enhancement coil enhances the coupling between the excitation coil-receiving coil and the test piece to improve the sensitivity of the receiving coil. The capacitance is connected in parallel to the passive enhancement coil to change the coupling. When the position of the excitation coil relative to the test piece has been determined, the capacitance becomes the only factor that affects the change of the inductance of the receiving coil in the sensor. Through experiments, the optimal capacitance value can then be determined.

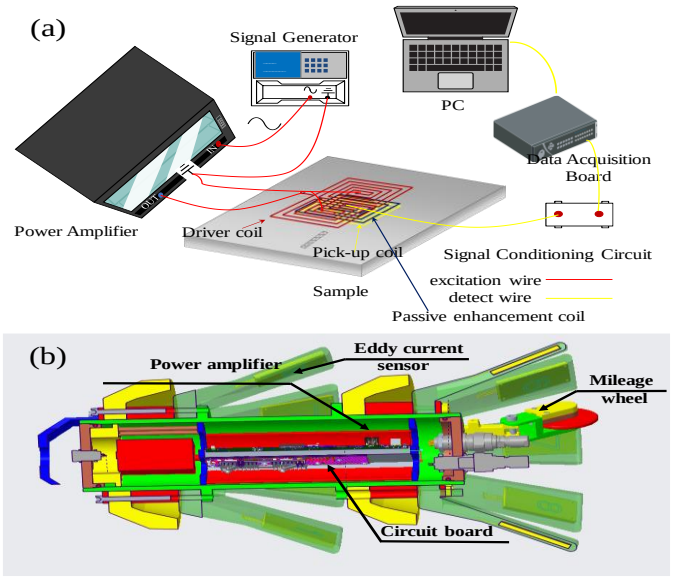

Fig. 1 (a) Testing system frame diagram, (b) Schematic diagram of an intelligent pig

When the sensor is placed close to the conductor, the eddy current occurs on the near-surface of the conductor. According to Lenz's law, eddy current in conductors produces opposite magnetic fields and it is hindering the change of the original magnetic field (Fig.2), where l denotes the lift-off, g is the gap between two layers. A new mutual inductance effect is generated between the excitation coil and receiving coil.

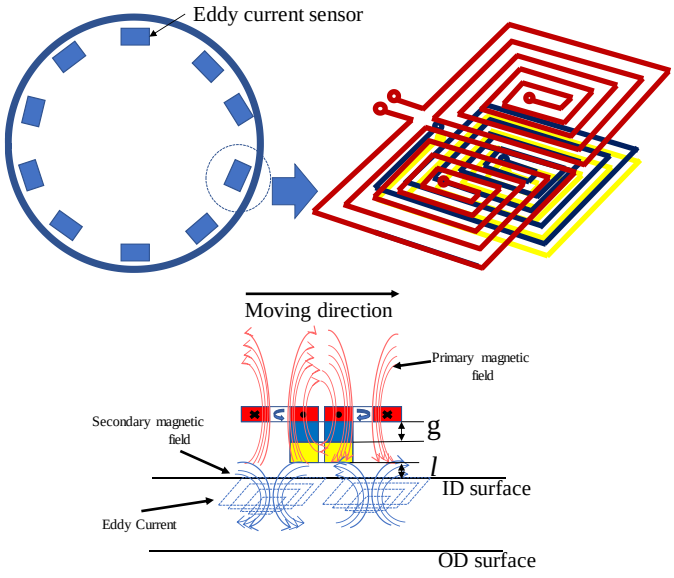

Fig. 2 Magnetic coupling between conductor and proposed probe

B. Analysis of the equivalent circuit

When a sinusoidal current flows through the excitation coil, an alternating magnetic field is generated. According to Faraday's law, the receiving coil will receive changes in magnetic flux and will generate induced electromotive force (EMF), which can be expressed according to [20] as

$$\varepsilon(t) = -\frac{d}{dt}\oiint_S B(x,y,z,t)\cdot dS \qquad (1)$$

where z is the thickness of the copper layer, S is the cross-section enclosed by the closed wire, B is the magnetic flux on the cross-sectional area, d is the line width and spacing. The induction of a planar coil in a magnetic field is simplified as a superposition of a rectangular coil, which is shown in Fig.3.

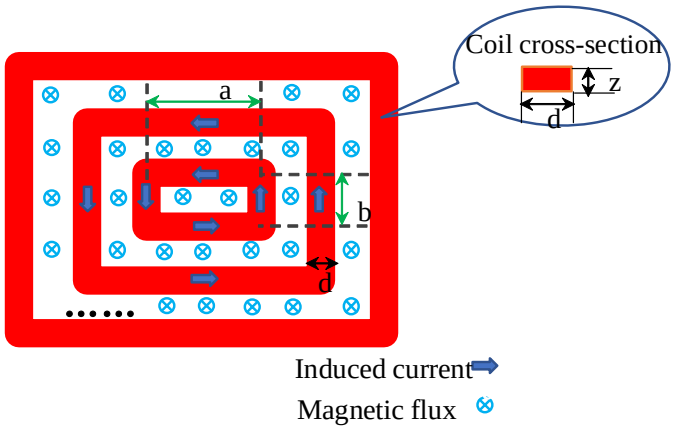

Fig. 3 Coil excitation field

Let B_i be the sum of the magnetic flux density through the area enclosed by loop i. B_i is the time-varying magnetic field generated by the coupling of the primary magnetic field and the secondary magnetic field. The induced voltage on the loops i is determined by Bi [21] According to Eq. (2), the induced voltage of the planar coil can be deduced in free space, namely

$$\varepsilon_i(t) = \frac{j\omega}{zd}\int_{Coil\ cross-section}\left(\int_{S_i}\hat{z}B_i dS_i\right)dArea \qquad (2)$$

where N is the number of turns of the coil, d is the wire width and spacing, Si is the area of the loop i, $\omega = 2\pi f$, in which f is the excitation frequency, $Area_i$ is the coil cross-section of the wire. Consider the coil parameters, the voltages can be deduced as: Defining a second-order vector A as it is given by $B = \nabla \times A$. Following the Stokes' theorem, Eq. (3) is expressed as

$$\varepsilon_i(t) = \frac{j\omega}{zd}\int_{Coil\ cross-section}\left(\int_{\Gamma_i}\hat{z}A_i dL_i\right)dArea \qquad (3)$$

where Γ_i is the circumference of loop i, which is determined by the a, b, and d. n is the number of turns of the pick-up coil. A_i is determined by the size and shape of the probe, the gap g between the detecting coil and the excitation, respectively. From Eq. (3), it is obvious that the induced voltages relate to the parameters of coil and excitation conditions [22]. To simplify the process, we employ circuit schematics for interpretation. The equivalent circuit diagram of the system is shown in Fig.4. To ensure the same magnetic field, the excitation coil requires applying the same voltage, where it is placed parallel at both ends of the power supply [22][23][24][25]. According to the Biot-Savart law, the magnetic flux relationship between the excitation and reception coils can be calculated, and Mutual inductance M can be solved by Neuman's formula [26] as

$$M = \frac{2\mu_0\sqrt{a\cdot c}}{\alpha}\cdot\left[\left(1-\frac{\alpha^2}{2}\right)K(\alpha)-E(\alpha)\right] \quad (4)$$

$$\alpha = 2\sqrt{a\cdot\frac{c}{[(a+c)^2+g^2]}} \quad (5)$$

where $2a$ and $2c$ are the diameters of two coils, g is the gap between two coils,

$$K(\alpha) = \int_0^{\frac{\pi}{2}} \frac{d\theta}{\sqrt{1-\alpha^2\sin^2\theta}} \quad (6)$$

and

$$E(\alpha) = \int_0^{\frac{\pi}{2}} \sqrt{1-\alpha^2\sin^2\theta}\, d\theta \quad (7)$$

are the first and second complete elliptic integrals, respectively. θ is the angle between the coils.

According to Equation (7), the mutual inductance is related to the parameters of the coil, and the gap g between the excitation and receiving coils plays an important role in the mutual inductance. That is to say, although the differential structure can suppress the effect of the primary magnetic field, the mutual inductance The effect can cause changes in the impedance of the detection coil, which can affect the detection results. Selecting the correct coupling spacing can improve detection lift-off and maintain sensitivity.

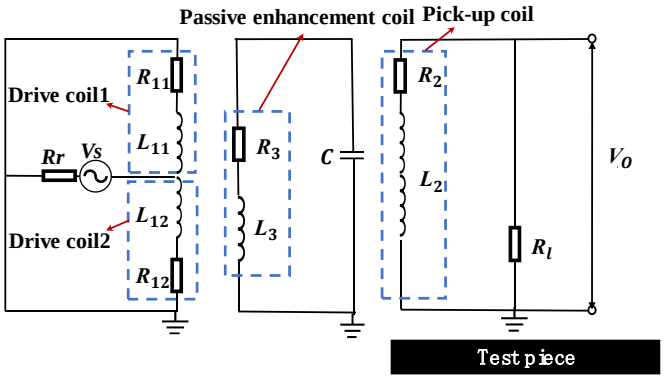

Fig. 4 Schematic diagram of the probe circuit

Vs is the input voltage, Rr is the internal resistance of the excitation device, R_{11}, R_{12} and L_{11}, L_{12} are the internal resistance and inductance of the two excitation coils respectively, R_2 and L_2 constitute the detection coil. C is the capacitor connected in parallel to the enhancement coil, and Vo is the output voltage. Thus, this data analyzed the differential coupled circuit with and without passive enhancement coil. For the convenience of analysis, the circuit diagram can be simplified into the following Fig.5(a) and (b), respectively[23][24].

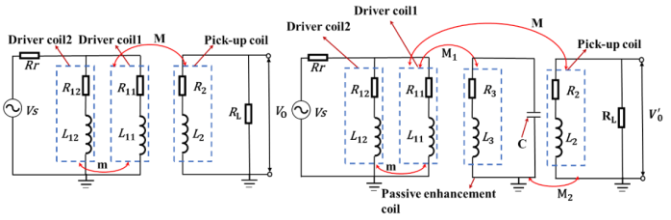

Fig. 5 The equivalent circuit of the probe (a) without passive enhancement coil and (b) with passive enhancement coil

According to Kirchhoff's law, the voltage depicted in Fig.5 (a) can be calculated as

$$\varepsilon_1(\omega) = -j\omega I_2 M \quad (8)$$

$$\varepsilon_2(\omega) = -j\omega(I_{11}-I_{12})M \quad (9)$$

$$Z_{11}I_{11} + j\omega I_{12}m + (I_{11}+I_{12})R_r - j\omega I_2 M = V_s \quad (10)$$

$$Z_2 I_2 - j\omega(I_{11}-I_{12})M = 0 \quad (11)$$

$$Z_{11}I_{11} + j\omega I_{12}m = Z_{12}I_{12} + j\omega I_{11}m \quad (12)$$

The optimized coil structure is shown in Fig.5(b), the voltage depicted in Fig.5(b) can be calculated as

$$\varepsilon_1(\omega) = -j\omega I_2 M \quad (13)$$

$$\varepsilon_2(\omega) = -j\omega(I_{11}-I_{12})M \quad (14)$$

$$Z_{11}I_{11} + j\omega I_{12}m + (I_{11}+I_{12})R_r - j\omega I_2 M - j\omega I_3 M_1 = V_s \quad (15)$$

$$Z_2 I_2 - j\omega(I_{11}-I_{12})M - j\omega I_3 M_2 = 0 \quad (16)$$

$$Z_{11}I_{11} + j\omega I_{12}m = Z_{12}I_{12} + j\omega I_{11}m \quad (17)$$

$$Z_3 I_3 - j\omega(I_{11}-I_{12})M_1 - j\omega I_2 M_2 = 0 \quad (18)$$

$Z_{11} = R_{11} + j\omega L_{11}$, $Z_{12} = R_{12} + j\omega L_{12}$, $Z_2 = R_2 + j\omega L_2$, $Z_3 = \sqrt{{R_3}^2 + (j\omega L_3 - \frac{1}{j\omega C})^2}$ represents the impedance of the driver coil, pick-up coil, and passive enhancement coil. Respectively, I_{11}, I_{12}, I_2 and I_3 are the current flowing through the excitation coils, the detection coil, and the passive enhancement coil, respectively. The term M is the mutual inductance between driver coil and pick-up coil. The m is the mutual inductance between two driver coils. M_1 is the mutual inductance between driver coil and passive enhancement coil and M_2 is the mutual inductance between passive enhancement coil and pick-up coil. Therefore, the output voltage V_O can be solved as

$$V_O = I_2 R_L = [j\omega M V_S(Z_{12}-Z_{11})R_L] \div [Z_2 Z_{11} Z_{12} + (Z_{12}+Z_{11}-2j\omega m)R_r Z_2 + (Z_{12}-Z_{11}+Z_2)\omega^2 M^2] \quad (19)$$

$$V_0' = [\omega^2 M_1 M_2 V_S(Z_{12}-Z_{11})R_L] \div [Z_3 Z_{11} Z_{12} Z_2 + (Z_{12}+Z_{11}-2j\omega m)R_r Z_3 Z_2 + (Z_{12}-Z_{11}+Z_3)Z_2\omega^2 {M_1}^2] \quad (20)$$

$$V_1 = V_0 + V_0' \quad (21)$$

Fig.5 shows that the place of the passive enhancement coil between the excitation coil and the receiving coil. This can increase the coupling between the excitation coil and the receiving coil, thereby improving the detection sensitivity.

From Eq.(22), when changing the capacitance of the receiving coil in parallel, the impedance of the receiving coil can be changed to affect the sensitivity of the detection. As long as the probe is placed close to the conductor, the mutual inductance M will be affected by the mutual inductance between the specimen and the coil. $M' = M + \Delta M$, this represents the mutual inductance affected by the sample and the parameters of coils. $Z' = Z + \Delta Z$, it is defined as transfer impedance that is influenced by the condition of the sample. If the sample has defects near the surface, the bias of impendence between two driver coils will lead the V_O over zero.

III. EXPERIMENTAL SETUP

A. Numerical simulation

To verify the detection capability of the probe structure, finite element simulation models are established in COMSOL Multiphysics software. This study mainly directs at the sensitivity of the new probe for detectability under high lift-off

impact. The 3D model in the software is used to construct the proposed probe. The computational complexity of the model is reduced by using meshes with different densities for different regions. Especially, frequency domain analysis is used to analyze models. All the flaw detection simulation experiments on flat plates and pipes are implemented under the magnetic field module.

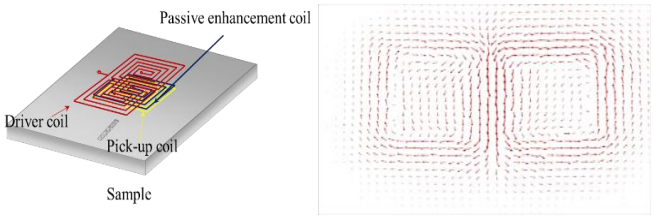

Fig. 6 (a) A model diagram of the probe, (b)Finite element simulation of eddy current field of the probe

The schematic diagram of the simulation model view is shown in Fig. 6(a). Specifically, the spiral coil is made of copper, and the simulated size model configuration is shown in supplementary material. The wire diameter of the excitation coil is 0.254 mm, the wire diameter of the passive enhancement coil and the receiving coil are both 0.0889 mm. In these simulation experiments, the voltage is set to 10V while the excitation frequency is set to 1MHz. The results of defect detection are obtained from the inductive voltage of the detection coil. In addition, the eddy current distribution diagram is shown in Fig. 6(b). The proposed structure forms a symmetrical eddy current field. In particular, the uniform field distribution will be generated in which has a positive influence on the detection. It is expecting to obtain maximum disturbance of eddy current once defects exist. Thus, the uniform eddy current field has obvious advantages in defect detection. The symmetrical excitation of the plane rectangular coil is used to generate a more uniform eddy current field on the pipe surface to improve the detection sensitivity

The distribution of eddy current in the non-defective area of the specimen is studied. The different defect characteristics in ferromagnetic specimens and pipe specimens were verified. In the experiment, 80# steel is ferromagnetic steel. The specific simulation details can be found in supplementary material.

B. Experimental validation

1)Experimental platform and inspection system: Fig. 7 illustrates the experimental verification for artificial defects detection and shows the detection of flat plate defects in a laboratory environment. The probe is connected by three separate layers of PCB. A specimen is produced to match with the simulation study while defects are made with different widths, heights, and shapes. The excitation mode is composed of the signal generator and power amplifier. The detection mode conducts the ADA4870 instrument amplifier to enhance the signal, and AD8302 is used to extract the induced voltage. After passing the low-pass filter, the NI-6226 data acquisition card is used for data acquisition. In the experiment, it is found that due to different material parameters and probe size, the results in the simulation can deviate slightly from the results in the experiment. Also, the experiment is affected by the speed effect which leads to the asymmetry of the signal acquisition. Similar to the simulation, the detection direction is divided into (A), (B), (C), (D) axes. The probe is clamped by the XYZ table, and the specimen is scanned in three directions. The detection speed is 20 mm/s and the lift-off value is controlled at a certain height with 5 mm, 7 mm, 9 mm, 11 mm respectively. Fig.9 shows the structure of the proposed Pipeline pigging system. It is implemented using FPGA based on direct digital frequency synthesis technology to generate a sine wave with adjustable frequency. The generated signal excites the excitation coil through the power amplifier ADA4870 and then receives the signal from the eddy current sensor through an analog-to-digital converter as well as generating a file record. The entire control process is controlled by STM32.

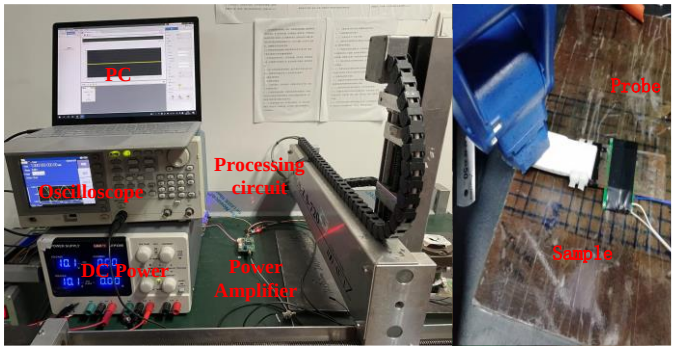

Fig. 7 Experiment platform and inspection system

The actual frequency used by the sensor is 1MHz. For determining this frequency, we simulate a detection situation of the sensor on the test piece by simulation of COMSOL Multiphysics software. The simulation is basically in line with the actual situation where individual sensors are shown to work simultaneously. All sensors work at the same time in order to comprehensively cover the pipeline. The test sample is 80# steel. Fig. 10(a) and Fig. 10(b) show the use of the internal detector to detect the internal defects of the whole pipe in a laboratory environment. The eddy current sensor array is packaged in the blade of the pigging while the hardware is placed in the cavity in the middle of the pigging. Fig.11 shows the structure of the proposed eddy current sensor.

A specimen is produced to match with the simulation study while defects are made with different widths, heights, and shapes as shown in Fig.8. Fig.12 shows natural corrosion pits and cracks. The depth of the pit is approximate 3 mm and the depth of the crack is around 1 mm. Fig.13 shows the artificial defects and welds inside the pipeline. Scanning is divided into three directions: A, B, C, and the sizes of defects (a-h) are $20\times40\times3$, $20\times3\times3$, r=2, $10\times2\times2$, $20\times10\times2$, $3\times10\times1$, $80\times40\times5$, $20\times40\times5$ mm^3, respectively. the pipe material is 80# steel.

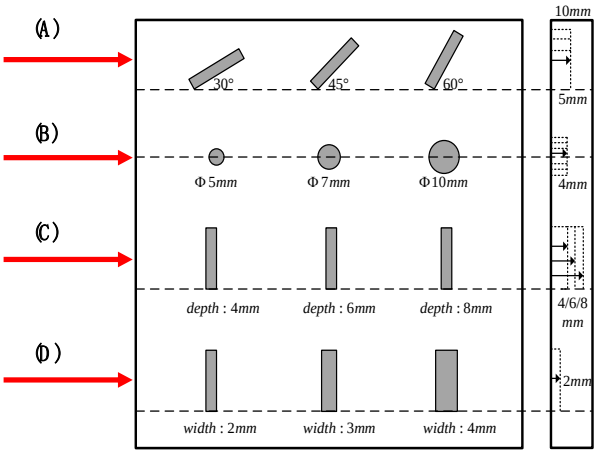

Fig. 8 Simulation of multiple defects under different lift-off conditions

Table I Parameters of simulation

Type of defect	Width change			Diameter change			Height change			Angle change		
	a1	b1	c1	a2	b2	c2	a3	b3	c3	a4	b4	c4
Length(mm)	10						10			10		
Width(mm)	4	3	2				2			2		
Height(mm)	4			4			8	6	4	4		
Angle(Compared to Y axis)	90°			90°			90°			60°	45°	30°
Diameter(mm)				10	7	5						

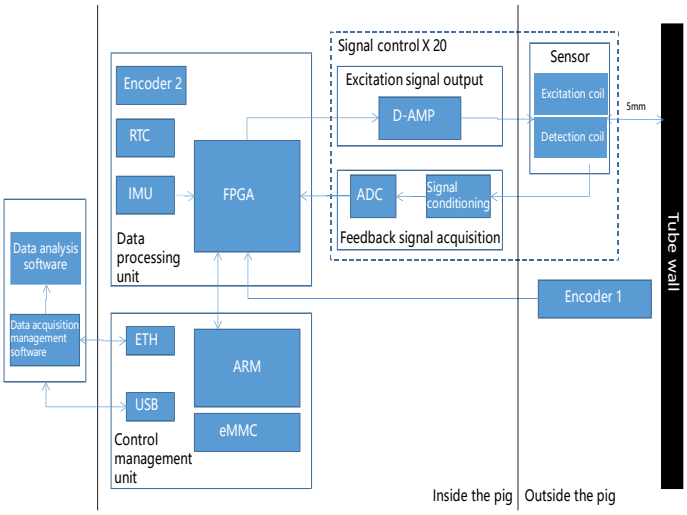

Fig. 9 Pipeline smart pigging system

Fig. 10 (a) Smart pigging, (b) the detection system for pipeline defects.

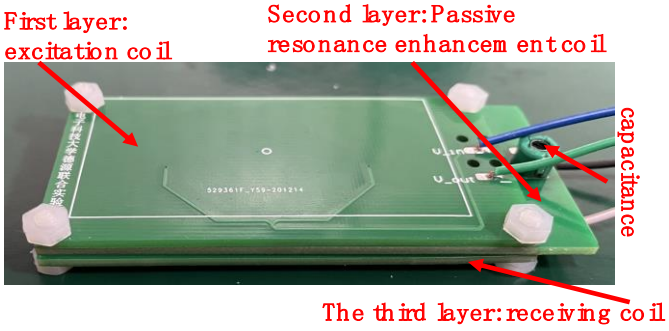

Fig. 11 The physical image of the sensor

Fig. 12 natural corrosion pits and natural corrosion cracks.

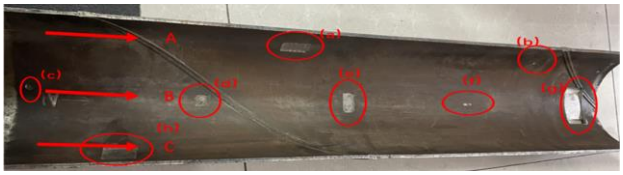

Fig. 13 (a), (b), (c) are the induced voltage of pipeline detection axis A, B, C with resonance enhancement

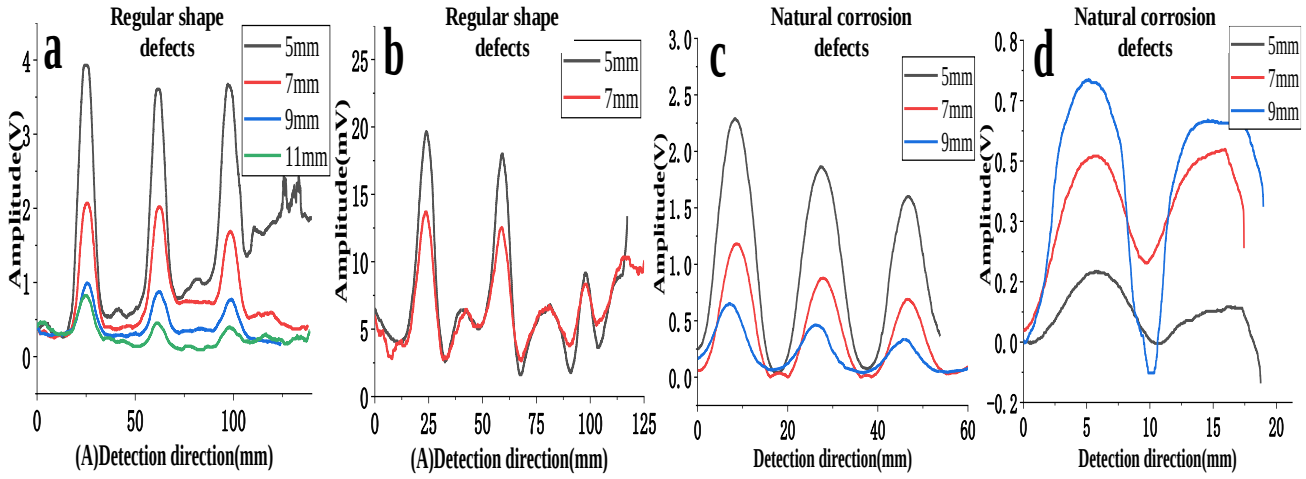

Fig. 14 (a). (b).Artificial defects detection axis A with resonance without resonance enhancement (c). (d)Corrosion pit and crack defect signal diagram

C. Experimental result analysis:

For eddy current testing, in order to quantitativly evaluate the detection sensitivity of the system, a parameter S is determined which is expressed as follows [27]:

$$S = \frac{|Max(V_{defect} - V_{normal})|}{Max(V_{normal})} \quad (22)$$

where S is the sensitivity of detection in the corresponding place, V_{defect} indicates the voltage value of coil probes when there is a defect, and V_{normal} means no defect.

Fig.8 shows the scan process by controlling the XYZ workbench under the same experimental conditions, different defects of the sensor without resonance enhancement and the sensor with resonance enhancement were tested at the same time. Fig.14 summarizes the detection results of the optimized sensor and the non-optimized sensor of the angular defect under different peeling values. Table II shows the S value of the detection results of different defects using optimized sensors and unoptimized sensors. ΔV1(v) is the voltage change of the optimized sensor. ΔV2(mv) is the voltage change of the unoptimized sensor. From Fig.14(a) and (b), it can be seen that there exists voltage fluctuations when scanning to defect and the voltage change of the optimized sensor is more noticeable than that of the unoptimized sensor. In addition, when there is an unoptimized sensor lifted by 7 mm, it becomes difficult to detect the defects. On the other hand, the optimized sensor is still able to detect defects even if it is raised by 11 mm in the same hardware configuration. Through the sensitivity comparison of Table II, the two sensors are more sensitive to depth defects. As the lift-off increases, the defect detection ability becomes weaker. In the case of 5 mm and 7 mm lift-off, the two sensors are more sensitive to the same defect. In terms of sensitivity comparison, the sensitivity of the optimized sensor has reached an average of 634%improvement.

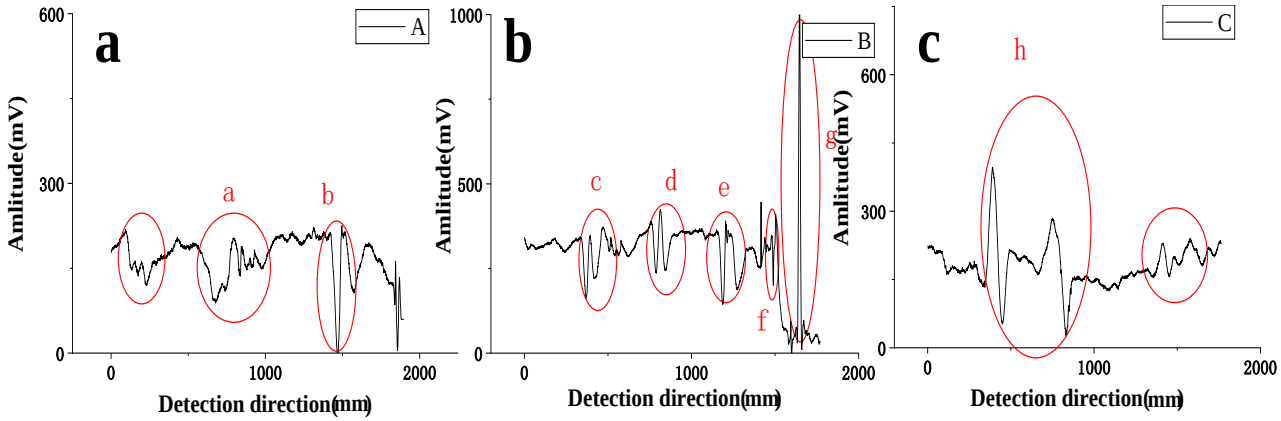

Fig. 15 artificial defects and welds inside the pipeline

Table II plate defect detection results

Parameters of defect			5mm		7mm		9mm		11mm	
			ΔV(v)	Sensitivity	ΔV(v)	Sensitivity	ΔV(v)	Sensitivity	ΔV(v)	Sensitivity
Angle of defect(mm)			3.7,3.0,2.8	18.6,14.0,13.1	1.9,1.4,0.7	9.3,6.9,3.7	0.8,0.6,0.4	4.0,1.8,1.0	0.6,0.1,0.06	3.1,0.6,0.3
30°	45°	60°								
Diameter of circular defect			3.3,2.2,0.9	16.5,11.2,4.6	2.6,1.04,0.32	13,5.2,1.6	1.8,0.1,0.2	8.8,2.0,0.2	0.8,0.05,0.2	4,0.3,0.8
5	7	10								
Height of defect(mm)			6.6,6.2,3.6	33.1,30.9,18.1	3.7,3.4,1.8	18.4,17,9.1	1.7,1.6,1.5	8.7,7.9,7.3	1.4,1.2,1.1	6.9,6.0,5.7
4	6	8								
Width of defect(mm)			5.4,4.9,3.8	27.1,24.7,19.5	2.5,2.4,1.9	12.4,11.9,9.6	1.0,0.8,0.6	4.9,3.8,3.0	0.9,0.5,0.4	4.7,2.3,1.8
2	3	4								
Natural corrosion cracking			0.7	6.3	0.4	4.1	0.1			0.9
Natural corrosion pit			2.2,1.8,1.5	21.8,17.5,14.9	1.1,1.1,0.6	10.8,11.4,5.9	0.6,0.5,0.2			5.5,4.9,2.3
1	2	3								

Enhancement of sensor detection capability by passive resonance effect was tested at the same time. Due to the relatively high lift-off value, the coil without resonance enhancement cannot detect defects on the existing hardware system.Fig.15(a-c) shows the sensor signal with resonance enhancement. The specific detection and analysis results are listed in Table III. The analysis shows that the unoptimized sensor has low sensitivity when the lift-off value is 1 cm and it cannot detect defects efficient enough. The optimized sensor, on the othetr hand, has better detection sensitivity. Therefore, the coil with resonance enhancement has a stronger detection ability than the coil without resonance enhancement, and several defective samples were tested to verify the effectiveness of resonance enhancement.

D. Comparison verification of pipeline defects:

In order to verify the advantages of the proposed probe, we compared the traditional U-shaped yoke probe and planar eddy current probe structures. The U-shaped yoke probe was designed referring to ACFM probes as reported in [28]. The planar probe was designed referring to EC probes as reported in [29]. The specific experimental setup is shown in Fig.16. Fig. 16 compares the detection effects of different internal detection methods on the internal defects of the pipeline. Due to the size and volume of the probes, they cannot be packaged and integrated into the current internal detector. Therefore, a robotic arm is used to support different probes to detect pipeline defects with the same parameters. Fig.16(a) shows that the probe is controlled by the 6-Axis Manipulator to scan the pipeline. The scanning speed is 20mm/s, and the scanning distance is 600mm. Fig.16 (c) shows the experimental state butter. In order to prevent clogging of the inner detector in the laboratory environment, butter is applied inside the pipe to increase the passage of the inner detector. Fig.16 (d) shows the inspection on the outside of the pipeline. Fig.16(b)(c)(d) shows 4 defects under different viewing angles, respectively. The parameters of different sensors are shown in Table IV. The metrics of different probes are listed in Table IV. The experiment is divided into the comparison of the detectability and sensitivity of the probe to different pipeline defects. By comparing different sensors, it is verified that the proposed sensor can achieve better detection capability at higher lift-off. This section actually discuss the impaction with different of lift-off distance.

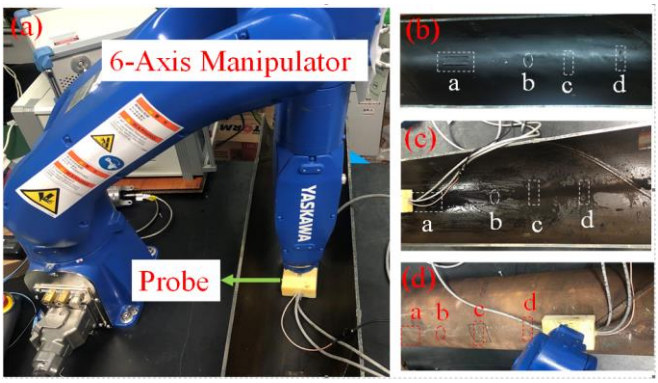

Fig. 16 Schematic of pipe inspection Testing system.

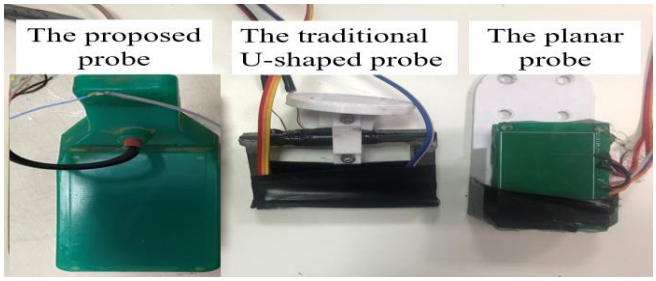

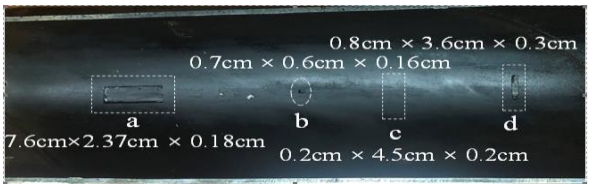

Fig. 17 (a) Probes structure (b)Pipeline defect distribution

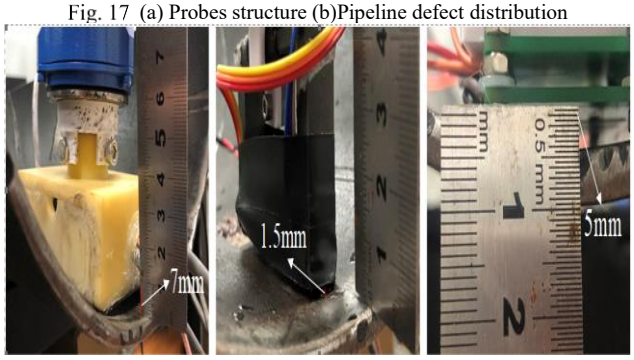

Fig. 18 Lift-off of different probes

Table III Pipeline defect detection results

defect	a	b	c	d	e	f	g	h
ΔV(mv)	95.4	192	172.6	103	200.7	130.2	860.8	221
Sensitivity	0.51	1	0.52	0.29	0.58	0.39	11.73	1.28

Table IV Comparison of the probes

The probes structure		The proposed probe	Traditional U-shaped yoke probe	Chen (2021)
Sensor		Coil	TMR	Coil
Excitation method		Coil	Yoke	Coil
Excitation frequency		1MHz	4kHz	2MHz
Turns		20	150	20
Length (mm)		48	67	48
Width (mm)		30	12	30
Height (mm)		11	44	10
Type and approximate size of Pipe Defects (mm)	The axial surface defect (a)	The square surface defect (b)	The circumferential sub-surface defect (c)	The circumferential surface defect (d)
	76×23.7×1.8	7×6×1.6	2×45×2	8×36×3

By comparing Fig.19 (a), Fig.19(b) and Fig.19(c), it can be observed that defects #a and #d on the inner side of the pipeline can be identified by all three probes. Defect #b can be detected by the proposed probe and planar probe through feature analysis. The traditional U-shaped probe cannot identify defect #b. The proposed probe can clearly identify the sub-surface defect #c while the planar probe fails to detect defect #b. The test results show that the proposed probe has high sensitivity and SNR in detecting small defects and sub-surface defects.

Table V comparison results

Probe type for pipe inspection	Proposed probe				Traditional U-shaped yoke probe				Chen (2021)			
Inner pipeline defect inspection	a	b	c	d	a	b	c	d	a	b	c	d
Sensitivity (Bz or Pcb coil)	1.7	1.3	0.2	1.5	1.1	0.04 0.3	0.2 0.9	1.0 1.1	1.9	0.51	0.03	0.64
Efficacy (Detectability)	D4/4				3/4				3/4			
Precise	√	√	√	√	√	×	√	√	√	√	×	√
Bz SNR (dB)	4.6	2.3	-14.0	3.5	6.9	-10	-0.9	0.83	5.6	-5.8	-30	-3.9

Note: √ and × indicates detected and not detected respectively

$$S = \left|\frac{Max(V_{Defect}-V_{(Defect-free)})}{V_{(Defect-free)}}\right| \quad SNR = 20\,log_{10}\left(\frac{V_{aD}}{V_{aN}}\right)[dB]$$

The evaluation is conducted by normalizing the experimental results due to the balance of different scale range of the different probe as shown in Eq. (23), and then solve the corresponding sensitivity. The results are shown in Table V.

$$Normalization = \frac{x-min(x)}{max(x)-min(x)} \quad (23)$$

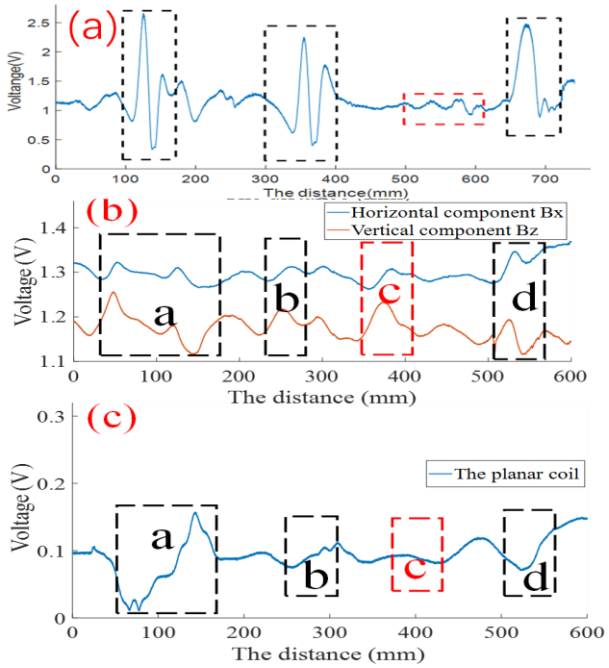

Fig. 19 Test results of different types of probes inside the pipeline. (a) The proposed probe. (b) The traditional U-shaped yoke probe. (c) The planar probe.

CONCLUSION

This paper has presented a design of an eddy current smart pig based on a sandwiched symmetrical differential planar probe. It is composed of an excitation coil, a passive resonance enhancement coil, and a detection coil. By comparing the coil without resonance enhancement and the coil with resonance enhancement, under the lift-off values of 5 mm and 7 mm, the sensitivity has reached an average of 634%, and the lift-off impact has been significantly resolved. In addition it has realized the detection of flat plate and pipeline defects about 1cm lift-off value. It has successfully detected surface micro-defects and corrosion defects with high sensitivity. Future work will focus on improving detection sensitivity, defect quantification, and the detection of both internal and external defects in the pipeline.

V. ACKNOWLEDGEMENT

The work was supported by Deyuan and UESTC Joint Research Center, supported by the National Natural Science Foundation of China (No. 61971093 and No. 61527803), supported by the International Science and Technology Innovation Cooperation Project of Sichuan Province: 2021YFH0036, Science and Technology Department of Sichuan, China (Grant No.2018JY0655 and Grant No.2018GZ0047)

REFERENCE

[1] Lu, H., Behbahani, S., Azimi, M., Matthews, J. C., Han, S., & Iseley, T. (2020). Trenchless construction technologies for oil and gas pipelines: State-of-the-art review. Journal of Construction Engineering and Management, 146(6), 03120001.

[2] Zakikhani, K., Nasiri, F., & Zayed, T. (2020). A review of failure prediction models for oil and gas pipelines. Journal of Pipeline Systems Engineering and Practice, 11(1), 03119001.

[3] Coramik, M., & Ege, Y. (2017). Discontinuity inspection in pipelines: A comparison review. Measurement, 111, 359-373.

[4] Tian, G., Gao, B., Gao, Y., Wang, P., Wang, H., & Shi, Y. (2016). Review of railway rail defect non-destructive testing and monitoring. Yi Qi Yi Biao Xue Bao/Chinese Journal of Scientific Instrument.

[5] Bickerstaff, R., Vaughn, M., Stoker, G., Hassard, M., & Garrett, M. (2002). Review of sensor technologies for in-line inspection of natural gas pipelines. Sandia National Laboratories, Albuquerque, NM.

[6] Ab Rashid, M. Z., Yakub, M. F. M., bin Shaikh Salim, S. A. Z., Mamat, N., Putra, S. M. S. M., & Roslan, S. A. (2020). Modeling of the in-pipe inspection robot: A comprehensive review. Ocean Engineering, 203, 107206.

[7] Kishawy, H. A., & Gabbar, H. A. (2010). Review of pipeline integrity management practices. International Journal of Pressure Vessels and Piping, 87(7), 373-380.

[8] Song, H., Yang, L., Liu, G., Tian, G., Ona, D., Song, Y., & Li, S. (2018, July). Comparative analysis of in-line inspection equipments and technologies. In IOP Conference Series: Materials Science and Engineering (Vol. 382, No. 3, p. 032021). IOP Publishing.

[9] Duan, Y. N., Han, Z. J., Li, G. Z., & Tian, H. (2012). Research on Key Technologies of the Cableless Pipeline Robot. In Advanced Materials Research (Vol. 591, pp. 1221-1224). Trans Tech Publications Ltd.

[10] Feng, Q., Li, R., Nie, B., Liu, S., Zhao, L., & Zhang, H. (2017). Literature review: Theory and application of in-line inspection technologies for oil and gas pipeline girth weld defection. Sensors, 17(1), 50.

[11] Papaelias, M. P., Lugg, M. C., Roberts, C., & Davis, C. L. (2009). High-speed inspection of rails using ACFM techniques. Ndt & E International, 42(4), 328-335.

[12] L. Yang, T. Guo, S. Gao, and B. Liu, "Feature analysis on magnetic flux leakage detection signals for special parts of oil and gas pipelines," *Journal of Shenyang University of Technology,* vol. 39, no. 01, pp. 43-47, 2017.

[13] Yamada, S., Katou, M., Iwahara, M., & Dawson, F. P. (1995). Eddy current testing probe composed of planar coils. IEEE Transactions on Magnetics, 31(6), 3185-3187.

[14] Fava, J. O., & Ruch, M. C. (2006). Calculation and simulation of impedance diagrams of planar rectangular spiral coils for eddy current testing. NDT & e International, 39(5), 414-424.

[15] Xu, P., & Shida, K. (2008, April). Eddy current sensor with a novel probe for crack position detection. In 2008 IEEE International Conference on Industrial Technology (pp. 1-6). IEEE. .

[16] Rosado, L. S., Santos, T. G., Ramos, P. M., Vilaca, P., & Piedade, M. (2015). A new dual driver planar eddy current probe with dynamically controlled induction pattern. Ndt & E International, 70, 29-37.

[17] Pasadas, D. J., Ribeiro, A. L., Ramos, H. G., & Rocha, T. J. (2016). Automatic parameter selection for Tikhonov regularization in ECT Inverse problem. Sensors and Actuators A: Physical, 246, 73-80. .

[18] Machado, M. A., Antin, K. N., Rosado, L. S., Vilaça, P., & Santos, T. G. (2019). Contactless high-speed eddy current inspection of unidirectional carbon fiber reinforced polymer. Composites Part B: Engineering, 168, 226-235.

[19] Caetano, D. M., Rabuske, T., Fernandes, J., Pelkner, M., Fermon, C., Cardoso, S., ... & Freitas, P. P. (2018). High-resolution nondestructive test probes based on magnetoresistive sensors. IEEE Transactions on Industrial Electronics, 66(9), 7326-7337. ”

[20] Desjardins, D. R., Krause, T. W., Tetervak, A., & Clapham, L. (2014). Concerning the derivation of exact solutions to inductive circuit problems for eddy current testing. NDT & E International, 68, 128-135.

[21] Fava, J. O., Lanzani, L., & Ruch, M. C. (2009). Multilayer planar rectangular coils for eddy current testing: Design considerations. Ndt & E International, 42(8), 713-720..

[22] Zhou, H., Zhu, B., Hu, W., Liu, Z., & Gao, X. (2014). Modelling and practical implementation of 2-coil wireless power transfer systems. Journal of Electrical and Computer Engineering, 2014.

[23] Ona, D. I., Tian, G. Y., Sutthaweekul, R., & Naqvi, S. M. (2019). Design and optimisation of mutual inductance based pulsed eddy current probe. Measurement, 144, 402-409.

[24] Xie, L., Gao, B., Tian, G. Y., Tan, J., Feng, B., & Yin, Y. (2019). Coupling pulse eddy current sensor for deeper defects NDT. Sensors and Actuators A: Physical, 293, 189-199. .

[25] Ona, D. I., Tian, G. Y., & Naqvi, S. M. (2019). Investigation of Signal Conditioning for Tx-Rx PEC Probe at High Lift-off Using a Modified Maxwell’s Bridge. IEEE Sensors Journal, 20(5), 2560-2569.

[26] Cheng, Y., & Shu, Y. (2013). A new analytical calculation of the mutual inductance of the coaxial spiral rectangular coils. IEEE Transactions on Magnetics, 50(4), 1-6.

[27] Yang, C., Gao, B., Ma, Q., Xie, L., Tian, G. Y., & Yin, Y. (2018). Multi-layer magnetic focusing sensor structure for pulsed remote field eddy current. IEEE Sensors Journal, 19(7), 2490-2499.

[28] Li Wei,Chen Guoming,Li Wenyan,Li Zhun,Liu Feng. Analysis of the inducing frequency of a U-shaped ACFM system[J]. NDT and E International,2011,44(3)..

[29] Chen K, Gao B, Tian G Y, et al. Differential coupling double-layer coil for eddy current testing with high lift-off[J]. IEEE Sensors Journal, 2021, 21(16): 18146-18155.

Yupei Yang received the B.Sc. degree from the University of Electronic Science and Technology of China (UESTC), Chengdu, China, in 2019. He is currently pursuing the M.Sc. degree in nondestructive testing using eddy current technique with the University of Electronic Science and Technology of China, Chengdu. His research interests include eddy current testing and wireless energy transfer.

Bin Gao (M' 12-SM' 14) received his B.Sc. degree in communications and signal processing from Southwest Jiao Tong University (2001-2005), China, MSc degree in communications and signal processing with Distinction and PhD degree from Newcastle University, UK (2006-2011). He worked as a Research Associate (2011-2013) with the same university on wearable acoustic sensor technology. Currently, he is a Professor with the School of Automation Engineering, University of Electronic Science and Technology of China (UESTC), Chengdu, China. His research interests include electromagnetic and thermography sensing, machine learning, nondestructive testing and evaluation where he actively publishes in these areas. He is also a very active reviewer for many international journals and long standing conferences. He has coordinated several research projects from National Natural Science Foundation of China. Personal web: http://faculty.uestc.edu.cn/gaobin/zh_CN/lwcg/153392/list/index.htm

Dong Liu received the B.Sc. degree in college of physics, Sichuan University, Chengdu, China, in 2004, the M.Sc. degree and the Ph.D. degree in control science and Engineering, University of Electronic Science and Technology, Chengdu, China, in 2010 and 2017, respectively. He is currently a research associate with the School of Automation Engineering, University of Electronic Science and Technology of China, Chengdu, China. His research interests include crystal oscillators, piezoelectric sensor and eddy current sensor.

Qiuping Ma received the B.Sc. degree in Electronic Information Engineering from Sichuan Normal University (2013-2017), Chengdu, China. She is currently pursuing the M.Sc. and the Ph.D. degree in nondestructive testing using eddy current technique at the University of Electronic Science and Technology of China, Chengdu, China. Her research interests focus on eddy current testing including near-remote filed eddy current testing and eddy current array.

Haoran Li received his B.Sc. degree in Electrical engineering and automation and M.Sc. degree in Control science and engineering from Southwest University of Science and Technology, Mianyang, China, in 2015 and 2018, respectively. He is currently pursuing the Ph.D degree at the University of Electronic Science and Technology of China, Chengdu, China. His research mainly focuses on eddy current testing and thermography as well as instrumentation manufacturing.

Wai Lok Woo (M'11–SM'12) received the B.Eng. degree in electrical and electronics engineering, and the M.Sc. and Ph.D. degrees in statistical machine learning from Newcastle University, U.K., in 1993, 1995, and 1998, respectively. He was the Director of research for the Newcastle Research and Innovation Institute, and the Director of operations for Newcastle University. He is currently a Professor of Machine Learning with Northumbria University, U.K. He has published more than 400 papers on these topics on various journals and international conference proceedings. His research interests include the mathematical theory and algorithms for data science and analytics, artificial intelligence, machine learning, data mining, latent component analysis, multidimensional signal, and image processing. He is a Member of the Institution Engineering Technology. He was a recipient of the IEE Prize and the British Commonwealth Scholarship. He serves as an Associate Editor to several international signal processing journals, including IET Signal Processing, the Journal of Computers, and the Journal of Electrical and Computer Engineering

Gaige Ru received the M.Sc. degree in control science and engineering from the Anhui Polytechnic University Wuhu, China, in 2019. He is currently pursuing the Ph.D. degree with the University of Electronic Science and Technology of China, Chengdu, China. His research mainly focuses on eddy current testing and magnetic flux leakage testing and instrumentation manufacturing. His research interests include smart sensors and system design for pipeline inspection.